Rev. Adv. Mater. Sci. 51 (2017) 35-49

GRAPHENE QUANTUM DOTS: THEORY AND EXPERIMENT

Mikhail F. Budyka[1], Elena F. Sheka[2] and Nadezhda A. Popova[2]

[1]Institute of Problems of Chemical Physics of RAS, Chernogolovka, Russia
[2]Peoples' Friendship University of Russia, Moscow, Russia

Received: April 20, 2017

Abstract. The current paper presents a consolidated view on empirical and virtual realities related to photonics of graphene quantum dots (GQDs). Empirically, the term is related to liquid and/or solidified dispersions of stacked nanosize framed graphene sheets/molecules, formed in due course of the circumference polyderivatization thus retaining sp^2 electron configuration of carbon atoms in basal plane. Predominantly, the framed molecules are presented by reduced graphene oxides (rGOs), largely varied by the framing chemical composition, size and shape. Placed in different surrounding, the molecules tend to form fractal structures thus still more strengthening inhomogeneity of the final GQDs. This size-content-shape-fractal inhomogeneity is the main factor governing the peculiarity of empirical spectral properties of GQDs. Virtually, GQDs photonics is attributed to individual framed molecules leaving the fractal inhomogeneity aside while focusing on chemical content only. However, a new important factor is met on the way that is related to open-shell character of electronic systems of framed graphene molecules. The feature is discussed in the paper by analyzing computed absorption spectra of a set of model molecules involving both framed sp^2 graphene and 'bulk' sp^3 graphene molecules, the latter resulted from the chemical modification occurred not only at the bare sheet circumference but at its basal plane as well. UHF ground states and ZINDO/S excited states of the molecules were analyzed. The UHF-ZINDO/S combination is well coherent in the case of 'bulk' closed-shell molecules for which UHF and RHF ground state results are identical. In the case of open-shell molecules, the incoherence of the UHF and ZINDO/S approaches is revealed in a considerable decreasing of the HOMO-LUMO energy gap provided by the restricted character of ZINDO/S formalism. The feature leads to drastic unrealistic red shift of absorption spectra, strongly contradicting experimental reality relevant to GQDs. Since GQDs photonics is a largely extending area, the development of feasible computational tools to describe excited states of large open-shell molecules is highly requested.

1. INTRODUCTION

Graphene exclusive peculiarities clearly exhibit themselves in its photonics involving optics and spectroscopy related to Raman scattering, photoluminescence, photochemistry, nonlinear optics, to name a few. Particularly, it concerns Raman scattering (RS) and photoluminescence (PL), which are the most demanded among other spectroscopic events. The former confidently takes place as the most required testing techniques and is widely used. Important, that Raman spectroscopy is equally applicable to graphene in each form. Oppositely, PL is inherent only to certain forms of graphene known as graphene quantum dots (GQDs). It is connected with the fact that macroscopic graphene crystal does not fluoresce due to the lack of energy gap in its electron spectrum. However, graphene sheets of nanometer size emit light in the visible region of the spectrum due to opening the gap. This clearly evi-

Corresponding author: Elena F. Sheka, e-mail: sheka@icp.ac.ru

dent effect of quantum confining stimulated the attribution of nanosize sheets to quantum dots and then to graphene quantum dots (GQDs).

Originally, the term appeared in theoretical researches and was attributed to fragments limited in size, or domains, of a single-layer two-dimensional graphene crystal. The issue concerned quantum confining manifested in the spin [1,2], electronic [3], and optical [4–9] properties of the fragments. Among the latter, GQDs turned out quite efficient fluorescent nanocarbons and became the most popular. Due to PL stability, nanosecond lifetime, biocompatibility, low toxicity, and high water solubility, the GQDs are considered excellent applicants for high-contrast bioimaging and biosensing applications. The latter stimulated the growth of interest in GQD, which rose the question of their mass preparation. Meeting this demand, a lot of synthetic methods appeared to produce GQDs, both "top down" and "bottom up." The former concern techniques such as electrochemical ablation of graphite rod electrodes, chemical exfoliation from the graphite nanoparticles, chemical oxidation of candle soot, intensive cavitation field in a pressurized ultrasonic batch reactor for obtaining nanosize graphite further subjected to oxidation and reduction. Laser ablation of graphite and microwave-assisted small-molecule carbonization present bottom-up techniques. These and other methods are widely used in the nowadays studies concerning GQD PL (see Refs. [10–13] and references therein) and are described in a number of reviews [14,15]. However the GQD technology is still costly and time consuming due to which working on efficient techniques getting GQDs in grams-mass quantities and searching cheap raw materials, chemists have turned to natural sources of carbon in the form of carbon fibers [16] and coal [17]. However, the biggest progress is evidently connected with shungite carbon [18].

In spite of large variety of techniques as well as difference in the starting materials, numerous studies exhibit a common nature of fabricated GQDs. The performed analysis of structure and chemical composition shows that in all the cases, GQDs are a-few-layer stacks of not bare but framed nanographene sheets, mainly, reduced graphene oxides (rGOs), of 1–10 nm in lateral size. There is only one observation when single-layer rGO domains were synthesized in a liquid medium using trialkylphenyl polymers that form three-dimensional pores [19]. In all other cases, the studied rGO stacks are highly varied: they differ by the number of layers and lateral dimension of the sheets as well by chemical composition of the latter. Thus, quasi-planar basal planes of the sheets are framed quite differently with respect to chemical units that terminate the sheets' edge atoms: C=O, C–C (COOH), C–OH, and C–H units are considered as main terminators. The terminator set has a direct connection with the graphene oxide (GO) nature of the parent species. As shown, a specific distribution of the latter over the sheets' circumference depends on the synthetic method used for the dot production. In its turn, it determines the solubility of GQDs in water and other solvents as well as a strong dependence of the GQDs PL properties on the solvents in use, thus making the size-content-solvent dependences the main features of the GQDs PL spectra. This is due to the fact that the GQD gap engineered by quantum confinement depends on the chemical modification of graphene edges as well as on size and shape of graphene fragments [20-26] and explains a large dispersion of PL properties that are affected by the synthetic method in use. This results in a large polydispersity of synthetic GQDs solution and accounts for excitation-dependent PL shape and position. Standardization of both size and chemical framing of nanographene fragments is a very complicated problem, and not so many successful results are known. Controlled synthesis was realized in the case of GDQs derived from carbon fibers [16], encapsulated and stabilized in zeolitic imidazolate framework nanocrystals [27], and under a particularly scrupulous keeping of the protocol of chemical exfoliation of graphite [11].

As mentioned earlier, a great hope in the production of a grams-mass GQDs material is pinned on the use of natural source of carbon. Impressive results of carbon-fiber-based [16] and coal-based [17] studies look quite promising. A particular feature of the studies concerned non-graphitic origin of both carbons, while the produced GQDs do not differ from those of graphite origin. Nevertheless, the natural carbons in the present case serve as raw materials for complex chemical synthetic technology of the GQDs production only. At the same time, Nature is infinitely generous to carbon and does not remain indifferent in this case as well. As if anticipating the need for quantum dots, Nature has prepared a particular natural deposit known as shungite carbon [18,28,29]. Its bright individuality, as expressed, in particular, in the total absence of any similarity to other natural carbon allotropes, put shungite carbon in a special position and formed the basis of more than half a century of careful study of its properties. The presence of sp^2 domains was one of the first observations. However, it took many years to establish the domains' nature. Stimulated

by the current graphene chemistry, both highly extensive empirically and deeply understood theoretically, the shungite study received a new impetus, which resulted in a new vision of this carbon [18]. At present, shungite carbon is considered as a multilevel fractal structure, which is based on nanoscale rGO fragments with an average linear dimension of ~1 nm. The fragments are grouped in 3–5 layer stacks, thus forming the second-level stacked structure; the stacks form the third-level globular structures of 5–7 nm in size, while the latter aggregate forming large nanoparticles of 20–100 nm. Experimental evidence of the structure has been recently proved by a detailed HRTEM study [29]. These data are well consistent with both X-ray and neutron diffraction studies [28,30]. A convincing proof of the grains' attribution to rGO fragments as well as their chemical composition describing the atomic C:O:H ratio of 11:1:3 was obtained in the course of inelastic neutron scattering study [31]. The latter has been confirmed by X-ray microanalysis [29]. The next-level structure elements related to stacks, globules, and large aggregates were reliably fixed as well. Once stacked, globulized, and aggregated in solids, rGO fragments are readily dispersed in water and other solvents forming colloidal solutions with their own multilevel structures.

Evidently, the multilevel structure, directly revealed for shungite carbon, is characteristic for synthetic GQDs as well. This makes the determination of what are GQDs quite uncertain while few-layer stacks is a widely accepted nowadays vision of synthetic dots. However, it is obvious that not stacks themselves, but rGO fragments (or other framed nanographenes) determine PL properties of GQDs. Apparently, it would be better to attribute GQDs to these very fragments, which will allow for considering their properties in view of large experience of molecular spectroscopy. On the other hand, such an approach opens a possibility to trace the influence of the fragment aggregation on PL properties by comparing the spectra behavior of GQDs under different size-content-shape-fractal inhomogeneities.

2. GRAPHENE QUANTUM DOTS: GENERAL CHARACTERISTICS

Optical spectroscopy and PL, in particular, becomes the primary method of studying the spectral properties of GQDs. Reviews [15,33] allow suggesting a synopsis of the general picture based on the study of synthetic GQDs, which can be presented by the following features:

- GQDs as objects of numerous studies present dispersions of nanosize framed graphene molecules in different solvents.
- The position and intensity of the GQDs PL spectrum depend on the solvent; the constituent graphene molecules are readily soluble in water and many polar organic solvents; in the transition from tetrahydrofuran to acetone, dimethyl formamide, dimethyl sulfide, and water, maximum of the PL spectrum is gradually shifted from 475 to 515 nm, which evidently manifests the interaction of the graphene molecules with the solvent.
- The PL intensity depends on the pH of the solution: being very weak at low pH, it increases rapidly when the pH is from 2 to 12, wherein the shape of the spectrum does not change.
- An important feature of the GQDs PL is the variation of its quantum yield in a wide range (from 2% to 46%); furthermore, this variation is associated not only with different ways of GQD production but is typical of the samples prepared by the same procedure; the PL quantum yield varies with time after synthesis.
- Both GQDs absorption and PL spectra show the dependence on size of basic graphene molecules and shift to longer wavelengths when size increases.
- The PL spectrum depends on the excitation wavelength λ_{exc}; with increasing λ_{exc}, the PL spectrum shifts to longer wavelengths and its intensity is significantly reduced.
- The PL mechanism is still unclear, despite a large number of proposed models and active experimental studies.

A detailed description of these features with the presentation of their possible explanations and links to the relevant publications is given in Refs. [15,32,33]. Fig. 1 summarizes the above said and presents a general view of spectral properties of GQDs water dispersions, which is characteristic for synthetic GQDs of different origin.

3. FRACTAL NATURE AND STRUCTURAL INHOMOGENEITY OF GQD DISPERSIONS

The GQD concept evidently implies a dispersed state of a number of nanosize graphene fragments, below empirically dominated by rGOs for simplicity, in a solvent. Once dissolved, the fragments unavoidably aggregate forming colloidal dispersions. It was suggested [34,35] that the formed colloidal aggregates can be attributed to fractals due to, first, the rGO sheets unavoidably involve elements of randomness in the course of both laboratory chemical re-

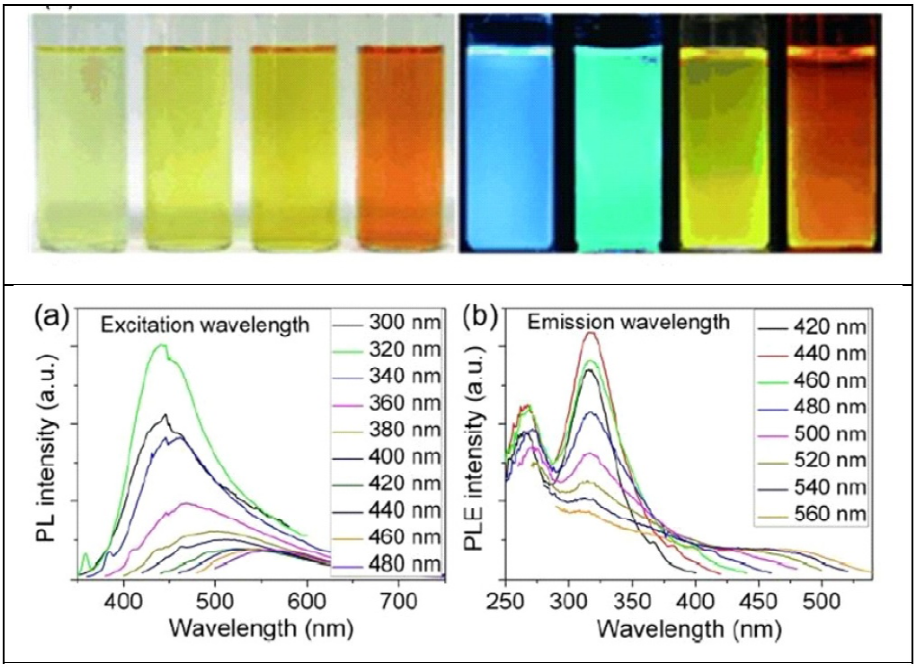

Fig. 1. Typical sized GQDs optical images illuminated under white (left; daylight lamp) and UV light (right; 365 nm) (top); PL spectra at different excitation wavelength (a) and PL excitation spectra at different emission wavelength (b) of water dispersions at room temperature of synthetic rGO obtained by solvothermal reduction. Adapted from Refs. 32 and 33.

actions and natural graphitization [29]; the latter concerns their chemical content, size and shape. Second, the sheets' structure certainly bears the stamp of polymers, for which fractal structure of aggregates in dilute dispersions has been convincingly proven (see Ref. [36] and references therein). Actually, the structure of colloidal aggregates is highly sensitive to the solvent around, the temperature of aggregate formation, as well as other external actions such as mechanical stress, magnetic and electric field. In addition to previously discussed, this fact imposes extra restrictions on the definition of quantum dots of colloidal dispersions at the structural level and strengthen previous suggestion of attributing GQDs to rGO fragments. In the case of the GQDs of different origins, the situation is even more complicated since the aggregation of synthetic (Sy) and shungite carbon (Sh) rGO fragments occurred under different external conditions. In view of this, it must be assumed that rGO-Sy and rGO-Sh aggregates of not only different, but the same solvent dispersions are quite different. Nevertheless, addressing spectral behavior of the dispersions, one should expect an obvious generality provided by the common nature of GQDs, while simultaneously complicated by the difference in packing of the dots in the different-solvent dispersions. The latter is clearly exhibited on the example of rGO-Sh dispersions [34,35]. Thus, the replacement of water with carbon tetrachloride (CTC) leads to a multiple growth of the pristine colloids, which promotes the formation of a quasi-crystalline image of the colloid aggregates structure. In contrast to CTC, toluene causes the decomposition of pristine water colloids into individual rGO fragments. The observed solvent-stimulated structural transformation is a consequence of the geometric peculiarities of fractals behavior in liquids [36]. GQDs-Sy were mainly studied in aqueous and some polar solvents without a detailed investigation of the relevant colloids composition.

The spectral behavior of the aqueous and CTC-dispersions with large rGO-Sh colloids is quite similar, despite the significant difference in size and structure of the latter. Moreover, the features of the PL spectra of these dispersions practically replicate patterns that are typical for the aqueous rGO-Sy dispersions. Specific effects of toluene, which caused the decomposition of water rGO-Sh colloids into individual rGO-Sh fragments with succeeding embedding them into toluene crystalline matrix, allowed for the first time to obtain the PL spectrum of individual rGO fragments. Obviously, the resulting fragments are of different size and shape, which determines the structural inhomogeneity of toluene dispersions. This feature of toluene dispersions is common with the other dispersions and explains

the dependence of PL spectra on λ_{exc}, which is the main spectral feature of GQDs, both synthetic [14,15,33,37] and of shungite carbon origin.

Besides the inhomogeneity, there is still one important factor that significantly complicates GQDs photonics. This concerns the interaction of dissolved rGO fragments with each other and with the solvent. All nanosize rGO fragments have high donor and acceptor properties (low ionization potential and high electron affinity) and can exhibit both donor and acceptor properties so that homoclusters of fragments (dimers, trimers, and so forth) are typical charge-transfer complexes. Besides this, some solvents, such as toluene in particular, are good electron donors due to which they can form a charge-transfer complex with any rGO fragment, acting as an electron acceptor. The spectrum of electron–hole states of the complex, which depends on the distance between the molecules as well as on the initial parameters, is similar to the electron–hole spectrum of clusters of fullerenes C_{60} themselves and with toluene [38–40], positioned by the energy in the region of 20,000–17,000 cm^{-1}. By analogy with nanophotonics of fullerene C_{60} solutions, the observed enhancement of the RS of toluene rGO-Sh dispersions [34,35] is due to the superposition of the scattering spectrum over the spectrum of electron–hole states, which follows from the theory of light amplification caused by nonlinear optical phenomena [41]. Additionally, the formation of rGO-solvent charge-transfer complexes may promote the formation of stable chemical composites in the course of photochemical reactions [42] that might be responsible for additional contribution to the observed PL spectra of GQDs dispersions.

4. OPTICAL SPECTRA OF OPEN-SHELL AND CLOSED-SHELL GRAPHENE-BASED MOLECULES

In contrast to extended experimental studies, computational consideration of GQDs spectral properties is rather scarce. One of the main reasons of the situation is the fact that rGO chemical complexity and uncertainty in size and shape inhibit the possibility of identifying a unique model structure representative of the species. However, the latest data, related to the spectra of individual rGO-Sh molecules [34,35,43] and supported by the data on their size and chemical composition [19,29-31], allow us to offer reliable rGO model molecules suitable for simulation of GQDs optical properties. The open-shell character of the molecules raises serious problems concerning computational tools in use. The first attempt to analyze this difficulty has been undertaken just recently [44] and is discussed in details in the current Section.

4.1. Objects under study

Generally, graphene-based molecules can be divided into three groups: (i) verily graphene (pristine) molecules presenting pieces of bare flat honeycomb sheets with non saturated dangling bonds of edge atoms; (ii) framed graphene molecules that are the molecules with fully or partially saturated dangling bonds in the circumference area; and iii) 'bulk' graphene molecules with chemical addends enveloping the whole body of the molecule carbon skeleton. The framed-and-'bulk' division reveals the unique two-zone feature of the chemical activity of pristine graphene molecules that governs the formation of any of their derivatives [45]. The extended computational experiment [44] was based on a set of model structures, adapted to the available spectral-structural information about rGO-Sh. Additionally, it covered a set of closed-shell GOs to reveal particular points of the excited states calculations, the most sensitive to the open-shell/closed-shell transformation. The two sets of model molecules are shown in Fig. 2. All the molecules are polyderivatives of the same parent (5, 5) NGr molecule, obtained in the course of stepwise hydrogenation [46] and oxidation [47] with different oxygen-based groups covalently bonded either to the edges only, thus matching a set of different rGOs, or also to the basal plane, thus transforming rGOs to GOs. Absorption spectra were the main subject of the study with an accent on the validity of computational tools traditionally used, about what may be judged by comparing the calculated and experimental spectra.

The (5, 5) nanographene (NGr) molecule in Fig. 2a presents a rectangle graphene sheet (55gr below) with bare edges involving five benzenoid units along both armchair and zigzag edges. Its 'chemical portrait' is shown in Fig. 2b as the atomic chemical susceptibility (ACS) image map [45,48]. The brightness of the image spots is proportional to the relevant ACS. As seen in Fig. 2b, the map clearly reveals two zones, namely, circumference covering edge atoms and basal plane, ACS of which, expressed via the number of effectively unpaired electrons on atom N_{DA}, differs more than four times in the favor of the former ones. Accordingly, the framing of pristine (bare) graphene molecules is the first stage of any chemical modification towards a complete polyderivatization. Since this reactivity area is

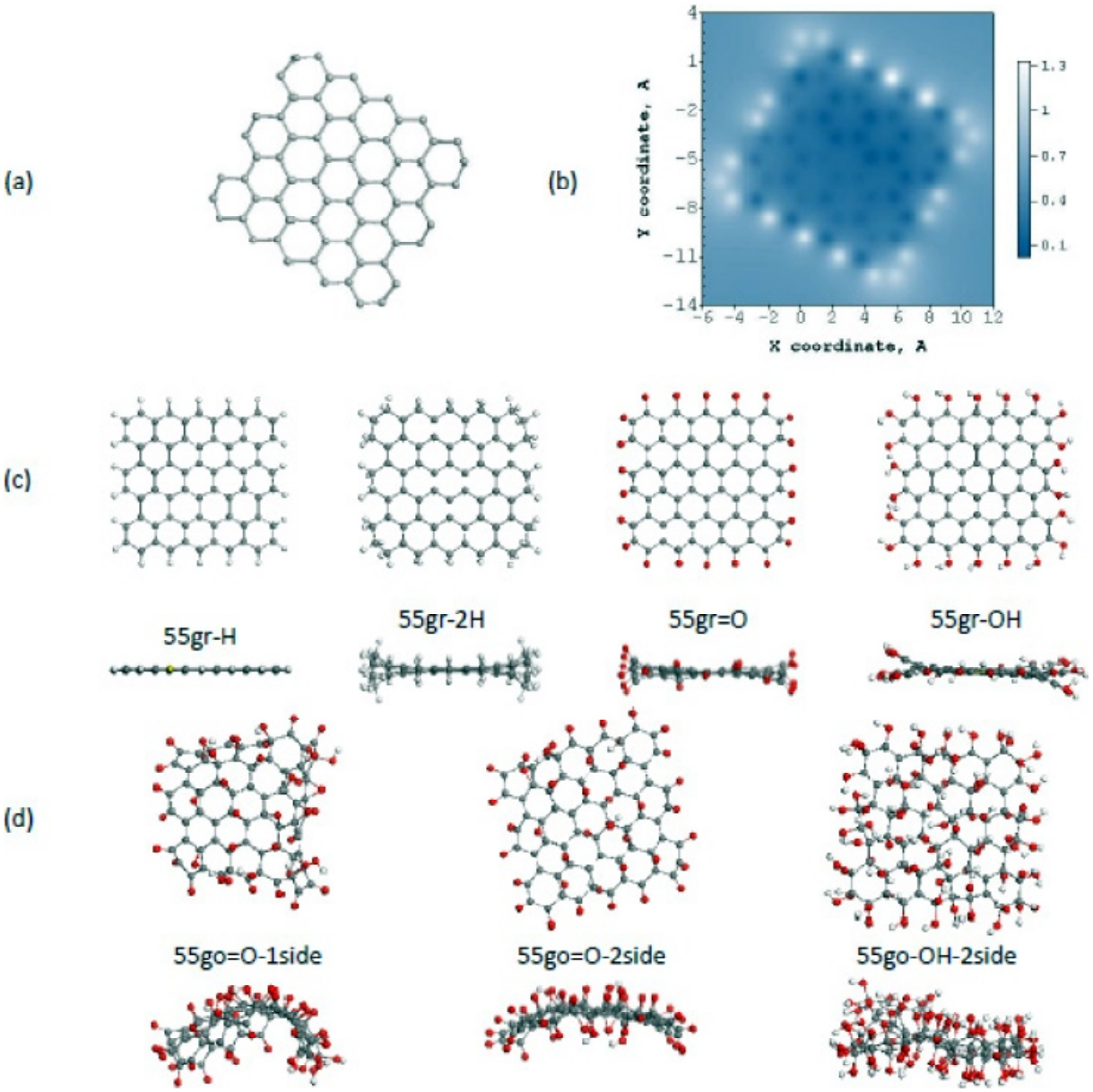

Fig. 2. Ball-and-stick representation of the equilibrium structures of graphene-based molecules models (top and side views). C atoms are depicted in grey, H in white and O in red. (a) Pristine (5, 5) NGr; (c) (5, 5) NGr molecule framed with (mono)(55gr-H) and (di) (55gr-2H) atomic hydrogen, atomic oxygen (55gr=O) and hydroxyl (55gr-OH); (d) Framed 55gr=O and 55gr-OH with epoxy (one- and two-side) and hydroxyl (two-side) units on the basal plane, 55go=O and 55go-OH, respectively. (b) Atomic chemical susceptibility N_{DA} image map over (5, 5) NGr molecule atoms in real space. Scale bar matches N_{DA} values. UHF AM1 calculations.

largely spread in space, the formation of the first monoderivative does not inhibit the molecule reactivity so that the reaction will continue until the reaction ability is satisfied. This means that any chemical modification of graphene starts as polyderivatization of the pristine molecule at its circumference. Consequently, involving basal plane atoms into reaction occurs usually at the second stage. The ACS image map in Fig. 2b evidences as well the open-shell character of the pristine 55gr molecule caused by the correlation of its p_z odd electrons [45]. The correlation extent is characterized by the total number of effectively unpaired electrons $N_D = \sum_A N_{DA}$. The linear size of the model of ~1 nm well suits the lateral size of rGO sheets in shungite carbon [29, 30].

The framed molecules in Fig. 2c correspond to the framing of the pristine molecule basal plane with C-H, C-2H, C=O, and C-OH units, which most often occur among the framing addends in reality. Among the models, 55gr-H molecule suits the best, both by size and chemical composition expressed as C_6H_2 content formula per one benzenoid unit, empirically studied rGO-Sh with content formula $C_6O_{0.1}H_{1.6\text{-}0.7}$ [29-31]. The molecule is an obvious favorite for comparison with experimental spectra similarly to that was discussed in [31] with respect to the inelastic neutron scattering (INS) spectra of shungite carbon. To clarify the dependence on the hydrogen content in the shungite formula 55gr-2H hydride was added to the rGO list. Beside the enhanced hydrogen content, the molecule, remaining open-shell one, still differs from 55gr-H by a complete valence saturation of the edge atoms. This inhibition of the circumference chemical activity is preserved when the rGO framing is made by oxygen atoms in the case of 55gr=O molecule while becoming again valence unsaturated in the case of 55gr-OH. Taking together, the molecules present a restricted set within an extremely large class of graphene oxihydrides forming rGOs of the 55gr-type. The quantum-chemical consideration of the variability of the rGO chemical composition is presented elsewhere [49].

'Bulk' molecules in Fig. 2d present three (5, 5) GOs formed in the course of the further monooxidant treatment of 55gr=O and 55gr-OH rGO molecules transferring them into 55go=O and 55go-OH [47]. The accessibility of the former molecule basal plane from either one or two sides results in different distortion of the carbon skeleton suggesting a new parameter effecting spectral properties of the molecules additionally to the effect of different oxidants. The side dependence is due to that the GOs carbon skeletons are formed by sp^3 configured atoms involved in the cyclohexanoid units of different isomorphic structures, which, in its turn, is responsible for peculiar bending of the pristine molecule basal plane presented in Fig. 2d [46, 47]. In contrast, skeletons of the framed molecules consist of sp^2 configured carbon atoms that still present compositions of benzenoid units, although with stretched C=C bonds.

4.2. Computational grounds

The model structures in Fig. 2 were obtained by using the AM1 version of semi-empirical unrestricted Hartree-Fock (UHF) approach. The approach, applied to closed-shell molecules, provides obtaining solutions fully identical to the RHF one [50], which allows considering a complete set of the models at the same computational level. Optical absorption spectra were computed in one-geometry-point mode for the equilibrium structures presented in Fig. 2 in the framework of the restricted Hartree-Fock (RHF) approach, by adopting the ZINDO/S model [51] implemented in Gaussian 09 package [52]. Up to 80 excited states were included.

ZINDO/S as well as other RHF techniques are well tested and widely used to compute the optical properties of large molecules (see Ref. 53 and references therein). However, the techniques is strictly applicable to closed-shell molecules only while the consideration of excited states of open-shell molecules requires more sophisticated configuration interaction (CI) approaches, such as coupled cluster singles and doubles model (CC2) [54], EOMCCSD and CR-EOMCCSD(T) [55], unrestricted algebraic diagrammatic construction (UADC) scheme of second order [56,57], UHF and UDFT calculations within the framework of the fragment molecular orbital (FMO) methods: (FMO-UHF) [58] and FMO-UDFT [59], respectively, as well as modified TD-DFT approaches [53,54,59,60]. Hartree-Fock based techniques are much preferable due to substantial errors from TD-DFT calculations of excited states of sp^2 carbon system [54]. All the mentioned CI techniques are time-consuming and hardly applicable to large systems. More promising are UADC and FMO-UHF approaches [57-59] but even these techniques are not efficient enough to perform an extended computational experiment similar to suggested for two sets of rGO and GO molecules so we have to restrict ourselves to the discussion of the results obtained by using ZINDO/S approach. A large pool of available experimental data on GQDs optical spectra provides a reliable comparison with computational results so it becomes possible to make conclusion about the reliability of ZINDO/S calculations related to closed-shell molecules and to reveal the method drawbacks with respect to the open-shell ones. The latter is of particular interest since this computational technique is widely used involving open-shell molecules as well.

5. COMPUTATIONAL RESULTS

5.1. HF peculiarities of the molecules ground state

As mentioned earlier, molecules shown in Figs. 2c and 2d are obtained in the course of stepwise hydrogenation [46] and oxidation [47] of the pristine (5, 5) NGr molecule. A restricted set of quantum

Table 1. Total number of effectively unpaired electrons and HOMO-LUMO energy gap.

No	Molecules	N_D, e	HOMO-LUMO energy gap		
			G_{UHF},eV	G_{RHF} [1)],eV	δG,%
1	(5,5)NGr(gr55)C_{66}	31.04	5.57	4.15	25.6
2	55hr-2$HC_{66}H_{44}$	12.23	6.35	3.10	51.2
	55gr-$HC_{66}H_{22}$	15.57	6.02	1.92	68.1
	55gr-$OC_{66}O_{22}$	16.02	5.81	2.94	49.4
	55gr-$OHC_{66}(OH)_{22}$	17.76	7.05	2.02	71.3
3	55go-2side-OH	0	8.43	8.43	0
	55go-1side=O	0	8.30	8.30	0
	55go-2side=O	0	8.26	8.26	0

[1)]One-point geometry calculations using UHF equilibrium structures.

chemical data of the studied molecules, related to the ground state but having a direct connection with the excited ones, is given in Table 1. As seen in the table, all the framed rGO molecules are characterized by nonzero numbers of effectively unpaired electrons N_D due to which they should be attributed to open-shell ones while the 'bulk' GO molecules are evidently closed-shell ones for which unpaired electrons are absent. The N_D value characterizes the correlation of p_z odd electrons of sp^2 systems and manifests their open-shell character. The energetic characteristics of the studied models involve the HOMO-LUMO gap values obtained in the course of the total optimization under UHF algorithm G_{UHF} and those calculated under RHF algorithm for equilibrium UHF structures G_{RHF}. The relative gap deviation $\delta G=(G_{UHF}-G_{RHF})/G_{UHF}$ marks changes in the HOMO-LUMO gap when going from UHF to RHF calculations at fixed molecular structure. As seen in Table 1, a drastic underestimation of the HOMO-LUMO gap G_{RHF} is observed when molecules become open-shell. The feature belongs to one of the common peculiarities of the optical spectra calculations if open-shell molecules are considered in the framework of restricted versions of either HF or DFT algorithms [55,58,59].

5.2. ZINDO/S excited states of GO closed-shell molecules

In the connection with the ground-state peculiarities discussed above, evidently, the results of the ZINDO/S calculated optical absorption spectra for open-shell and closed-shell molecules should be considered separately. First, closed-shell sp^3 molecules of GOs belonging to models shown in Fig. 2d will be considered. The correctness of the approach application is without doubt so that the matter is about how well the computation results fit experimental evidences. Fig. 3a presents a collection of calculated absorption spectra. As seen in the figure, the spectra are formed by optical excitation of different excited states presented by δ-bars and characterized by the location of the excitation on different atomic groups. Multiple internal and external factors, such as various structural and dynamic inhomogeneities discussed earlier, result in the broadening of the spectral shape in practice. This is usually taken into account via convolution of computed δ-spectra with Lorentzians of different full-width-half-maximum (FWHM) parameters.

Comparing spectra given in Fig. 3a, one can conclude that in all the cases they are located at high energy above 4 eV. This should be evidently expected due to sp^3 character of the molecule's carbon skeletons, which, as in the other numerous cases related to valence-saturated carbonaceous hydrooxides, provides absorption spectra located in the UV region [61]. The spectra exhibit a noticeable dependence on oxygen containing groups (OCGs) when substituting atomic oxygen, incorporated into carbonyls and epoxy units in the molecule circumference area and on basal plane of 55go=O species, respectively, by hydroxyls in the case of 55go-OH. Less but still significant changes are observed when oxidation concerns either one or two sides of the skeleton. Altogether, the picture presented in the figure allows predicting a considerable inhomogeneous background of the empirical spectra of GOs caused by the OCGs variation exaggerated by one-side or two-side adsorption. This conclusion well correlates with experimentally observed absorption spectrum presented in Fig. 3b for the GO aqueous dispersion at room temperature. Evidently, the main part of empirical spectrum is located in the UV region while tremendously broad-

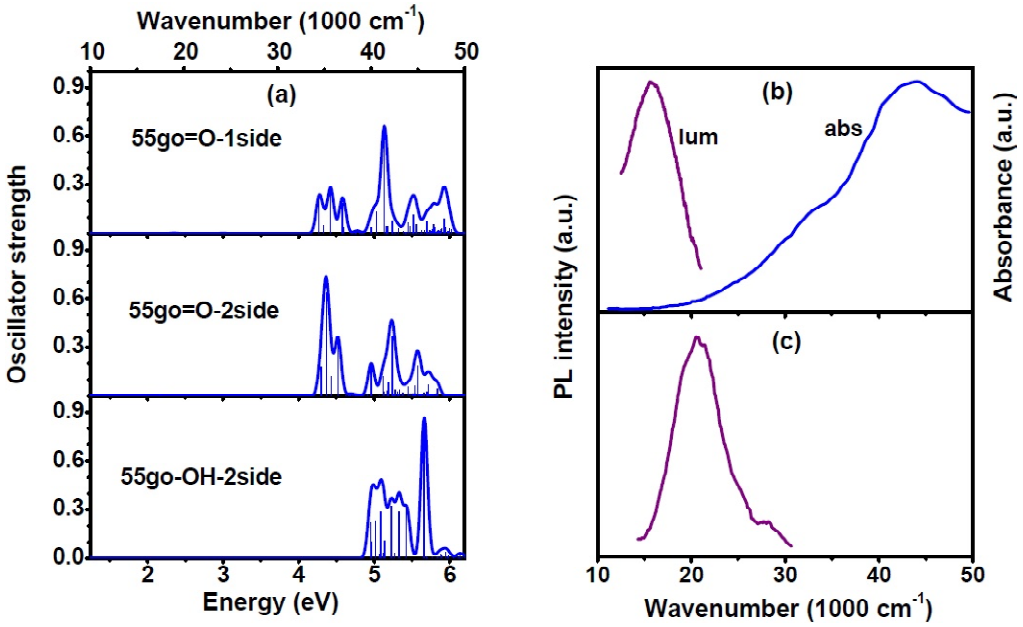

Fig. 3. (a) ZINDO/S optical absorption spectra of GO molecules 55go=O-1side, 55go=O-2side and 55go-OH-2side from top to bottom, respectively. Pristine δ-band spectra are convoluted with Lorentzian FWHM of 0.1 eV. (b) Absorption and fluorescence spectra of synthetic GO in water at room temperature; adapted from Ref. [62]. (c) Fluorescence spectrum of GO thin film at room temperature; adapted from Ref. [63].

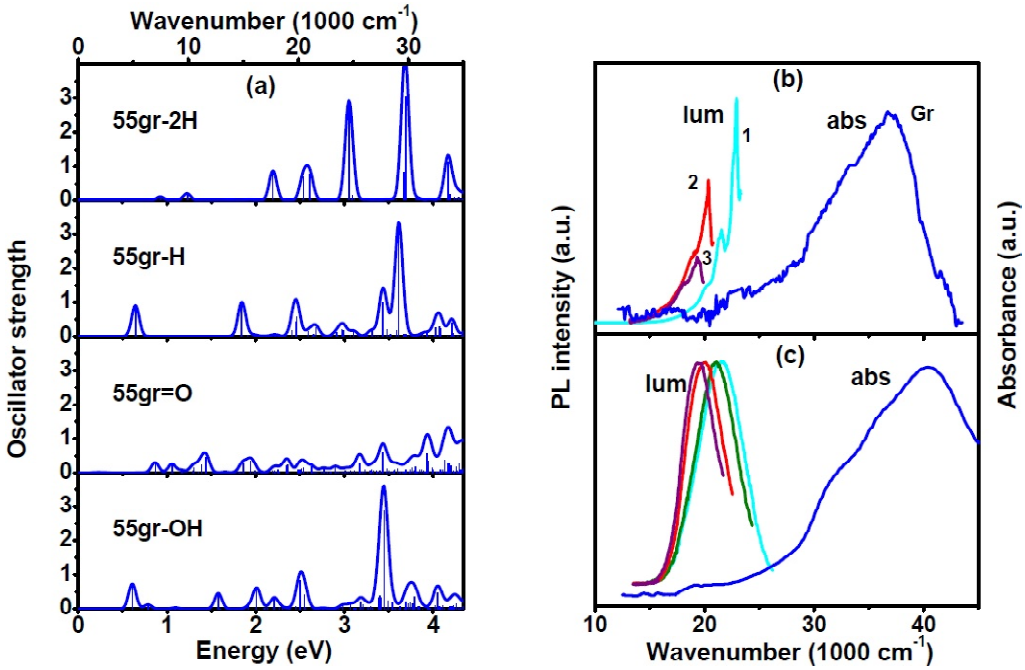

Fig. 4. (a) ZINDO/S optical absorption spectra of rGO molecules 55gr-2H, 55gr-H, 55gr=O, and 55gr-OH from top to bottom, respectively. Pristine δ-band spectra are convoluted with a Lorentzian FWHM of 0.1 eV. (b) Absorption spectrum of free standing monolayer graphene at room temperature; adapted from Ref. [65]. Fluorescence spectra of rGO-Sh in crystalline toluene matrix at 80K at different laser excitations: 405 nm (cian), 457 nm (red) and 476 nm (purple), respectively; adapted from Ref. [38] (c) rGO-Sy fluorescence spectra in different solutions: THF (cian); acetone (green); DMF (red) and water (purple) at room temperature; adapted from Ref. [64]. Absorption spectrum in the RPMI 1640 medium at room temperature, adapted from Ref. [66].

ened. Actually, the temperature effect constitutes a large part of the broadening while the remaining is still large thus providing the characteristic dependence of the GO fluorescence on the excitation wavelength due to selective excitation of different emitting centers inhomogeneously distributed over the sample [62-64]. This inhomogeneity was clearly observed in the inelastic neutron scattering spectra from different GO samples as well [31]. As for fluorescence spectra, once shifted at different excitations, they are located in visible region in the case of both aqueous dispersions [62] (Fig. 3b) and solid films [63] (Fig. 3c). As seen in Fig. 3, significant Stock's shift between the lowest bound of the excited states energy and fluorescence spectra position is observed.

5.3. ZINDO/S excited states of rGO open-shell molecules

Fig. 4a presents a collection of absorption spectra of four framed molecules shown in Fig. 2c. As in the previous case, the spectra are formed by optical transitions to a set of excited states differing by the location of the photoexcitations on the molecule's atomic groups. The pristine δ-spectra are Lorenzian convoluted by using FWHM of 0.1 eV. As seen in the figure, the obtained spectra drastically differ from those of GO molecules in Fig. 3a. Contrary to well grouped GO spectra within the region of ~2 eV in width, all the rGO spectra are largely extended, filling much broader interval of ~4 eV, including a deep IR region up to 5,000 cm^{-1}. Evidently, the feature is resulted from decreasing the energy gap between occupied and unoccupied orbitals discussed above. At the same time the calculated spectra are still sensitive to chemical composition of the studied molecules, which is obvious atomic property of spectra and should be reproduced by any atomic sensitive computational technique.

Presented in the right column panels of Fig. 4 are PL spectra of rGO-Sh in crystalline toluene matrix at T=80K at different excitation wavelength (Fig. 4b) and of synthetic rGO-Sy dispersed in different solution at room temperature (Fig. 4c). Additionally, Fig. 4b presents absorption spectrum of free-standing graphene macrosheet. The spectrum exhibits a molecular outline of the total absorbance after subtraction of a practically constant background, caused by peculiarities of the excitonic Fano resonance, from the experimental spectrum (see details in [65]). Actually, in the region of 10,000 – 30,000 cm^{-1}, the spectrum is well consistent with that of rGO-Sh in the CCL_4 solution [38] as well as in a full spectral range of rGO-Sy presented in Fig. 4c [66]. As seen in Figs. 4b and 4c, the absorption of rGO molecules is located in a deep UV similarly to that one of GO molecules. In both cases the spectra are presented by spectral envelopes differing by the underlying constituents, which explains the shift in the position of spectra maxima. The evidence of UV absorption spectrum of rGO is well consistent with its PL lying in the visible region, as it was in the case of GOs. However, if empirical spectral properties of rGOs are well consistent, they strongly contradict the calculated data shown in Fig. 4a. Actually, for all the framed molecules, the low-energy bound of the computed absorption is lying in IR, which not only differs from the experimental spectra but excludes the PL observation in visible region oppositely to the situation related to the computed GO spectral features. The observed discrepancy has a serious reason which will be considered in the next section.

6. GENERAL REMARKS CONCERNING THE INTERRELATION BETWEEN EXPERIMENTAL AND CALCULATED OPTICAL SPECTRA OF GQDs

As previously, the discussion concerning the interrelation of calculated absorption spectra of GOs and rGOs with the empirical reality will be performed separately. Addressing GOs, one is facing a number of problems, the main of which is that the term *graphene oxide* covers an extremely large class of graphene polyderivatives, differing by chemical composition, size and shape. The last three factors significantly influence both absorption and fluorescence spectra (the effect related to the first factor is well shown in Fig. 3a) making them variable in a large spectral region due to which the GO spectroscopy is spectroscopy of structurally inhomogeneous samples characterized by remarkable broadening. The next complication arises from studying the GO spectra in solutions (mainly in water) at room temperature. These two circumstances significantly exaggerate broadening, complementing it by red-shifting. Therefore, no standard empirical GO spectrum can be suggested to provide its correct comparison with a calculated one attributed to a fixed molecular structure at a quantitative level. One may operate with some average image of experimental reality only and look about the support of general tendencies. From this viewpoint, the situation with GO spectroscopy looks quite positive. According to

experimental evidences [62-64], the GO absorption spectra are located in the UV-vis region and consist of an intense maximum at 250-400 nm (4.96-3.10 eV) followed with long-wavelength tail up to near IR (Fig. 3b). Evidently, the maximum should be attributed to intense excitations located above 4 eV in the calculated GO absorption spectra in Fig. 3a. As for the long-wavelength tail, a lot of experimentally provided complications may be suggested to explain its existence. Important issue is that there is no strong absorption in the visible region of GOs in practice that is in consent with calculated data. Similarly to absorption, the PL spectrum is quite variable as well, nevertheless, presented by a single broad band. The band maximum position varies from 365 nm to 605 nm (3.40-2.05 eV) [62,63,67-69] (see Figs. 3b and 3c), which is strictly connected with the object under study. The fact is well consistent with calculated spectra in Fig. 3a, according to which the emission should occur below 1.95-2.05 eV (530-500 nm) in the case of 55go=O-2side and 4.96 eV (250 nm) for 55go-OH-2side. A variable composition of the main OCGs, involving O, OH, and COOH units, alongside with different size of GO molecules is possible to explain the observed variability of the experimental spectra.

The empirical situation concerning optical spectra of rGOs is very rich and diverse (see reviews [15,32,38]). First of all, it is caused by a large variety of rGO species (see, to name but a few [15,40,67], on the one hand, and a pronounced diversity in experimental techniques and conditions (solvents, temperature, various external actions) used under GO reduction, on the other. Among this variety there was a place for an undeniable uniqueness – the presence of the rGO-Sh spectrum that can be attributed to a fixed molecule structure and thus considered as a standard spectrum. The uniqueness concerns fine structure fluorescence spectra of individual rGO-Sh molecules, fixed at low temperature in toluene matrix, whose size and chemical composition is well described by the gr55-H model discussed above [34,35]. This PL spectrum is presented in Fig. 4b at different excitation wavelengths. The spectrum collection reveals the possibility of selective excitation of different rGO-Sh molecules thus pointing to inhomogeneous mixture of molecules different by size. Actually, the conservation of the spectrum shape followed by red-shifting at increased excitation wavelength evidences a predominant influence of the molecule size.

Locally proved atomic content of rGO-Sh [29] is close to C_6H_2 characteristic for gr55-H, which gives right to take the gr55-H molecule as a reliable model responsible for the features of absorption and PL spectra presented in Fig. 4b. However, the comparison of virtual adsorption spectrum of the molecule in Fig. 4a with empirical reality presented in Figs. 4b and 4c reveals a drastic discrepancy caused by unreal red shift of the former. This spectrum position in IR not only contradicts to the UV position of the empirical spectra but fully excludes rGO PL in the visible region as well. Since such a drastic discrepancy is not characteristic for the computational technique in use, which was convincingly proven in the case of GO molecules discussed earlier, the observed feature should be attributed to the basic difference between GO and rGO molecules and be evidently connected with open-shell character of the latter. As mentioned in Section 5.1, RHF-based computational techniques, to which ZINDO/S belongs, produce underestimated HOMO-LUMO gap G_{RHF} of open-shell molecules. This is a common signature of the RHF approach bankruptcy in the case, evidenced for polyacenes [68] and presented in Fig. 5 for a set of coronene based models. As seen in the figure, the open-shell extent of the molecules progressively grows when n changes from 1 (benzene) to 5. Simultaneously, G_{RHF} strongly decreases while the difference between G_{RHF} and G_{UHF} becomes larger. Since the gap value determines the spectral range of the molecule absorption, obviously, the RHF-stimulated reduction of the HOMO-LUMO gap of open-shell molecules is obligatory resulted in the red shifting of absorption spectra. As for G_{UHF}, it changes much less when n increases, thus keeping value at the level of that for coronene and limiting the shift within UV and visible region. The data listed in Table 1 are coherent with the explanation. Actually, G_{UHF} of gr55-H is three times bigger than G_{RHF}. Practically, the same threefold changes are observed for all the rGO molecules. The difference should evidently result in a considerable blue shift of the absorption spectra with respect to the ZINDO/S calculations due to which the PL of the molecules should be observed in the visible region.

Among other governing factors, a gradual lowering of G_{UHF} when going from 55gr-H to 1111gr-H and 1512gr-H based on (11, 11) NGr and (15, 12) NGr molecules [69], is well consistent with red shift of empirical PL spectrum when the molecule size increases. In contrast, the dependence of excitation spectra on the chemical composition of the circumference framing of carbon skeleton of 55gr rGOs does not reveal straight tendency. In this connection, we cannot ignore numerous discussions of a special role of the states of edge atoms (see Ref.

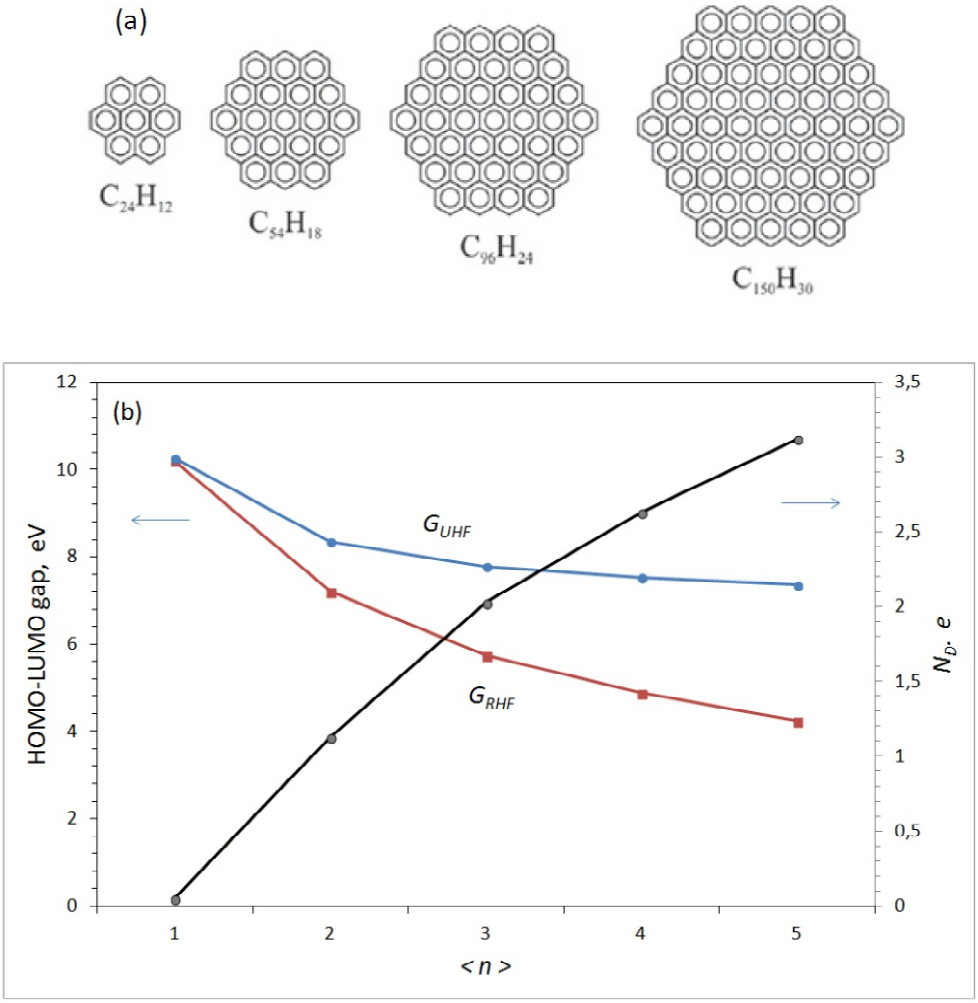

Fig. 5. (a) Equilibrium structure of coronene based molecules $C_{6n^2}H_{6n}$ for n=2, 3, 4, and 5. (b) G_{UHF} and G_{RHF} HOMO-LUMO gaps (left axis) and the number of effectively unpaired electrons N_D (right axis) as function of n. UHF AM1 calculations.

70 and references therein). In fact, this role is greatly exaggerated. Thus, in a series covering 55gr, 55gr-H and 55gr-2H molecules spin density on edge atoms changes drastically from 1.3-1.0 e in the parent 55gr (see Fig. 2b) to 0.42-0.22 e in 55gr-H and to zero in 55gr-2H due to complete saturation of the edge atom dangling bonds in the latter case. At the same time, G_{UHF} takes the values 5.57 eV, 6.02 eV, and 6.35 eV, respectively, not revealing the presence of any drastic effect. Another case, G_{UHF} changes from 6.02 eV to 5.81 eV when going from partially unsaturated to completely saturated dangling bonds in 55gr-H and 55gr=O, respectively, and then again reaches 7.05 eV in 55gr-OH with a partial unsaturation. It would seem that once important, saturated/unsaturated states of the edge atoms should strongly affect the electronic states of the molecules while in practice the changes are not tendentious but a strictly individual. One can confidently assume that extension of the current computational experiment by using either ADC [56] or UHF-FMO [58,59] formalism will allow clarifying the risen issues making the optical spectroscopy of open-shell molecules more transparent.

Evidently, the tree-fold lowering of G_{UHF} under transformation to G_{RHF} cannot be a universal law and may be a consequence of some other common properties of the studied molecules. Such an obvious common characteristic is a rectangular structure of the molecules of the second group with clearly formed armchair and zigzag edges. If the structure architecture is changed, so that the edges are not clearly determined as, say, it is in the case of polycyclic aromatic hydrocarbons $C_{24}H_{12}$ and $C_{114}H_{30}$ [70] or $C_{6n^2}H_{6n}$ in Fig. 5, the difference between G_{UHF} and G_{RHF} becomes less [69]. The finding is well consistent with a pronounced topochemistry peculiar to graphene structures in general [71], which allows suggesting a new topochemical effect of

graphene molecules exhibited in the dependence of their optical spectra on the molecule shape.

7. SUMMARY AND CONCLUSIONS

As follows from the discussed above, empirical spectral properties of rGO and GO molecules are practically identical due to which studies of GO photonics are often presented as GQD photonics thus producing a misunderstanding what GQDs are. Owing to a doubtless similarity in the spectral behavior of synthetic rGO-Sy and natural rGO-Sh graphene quantum dots, the findings for rGO-Sh can be generalized and presented as attributed to the whole GQDs class. Accordingly, the photonics of GQDs faces the problem that a large statistical inhomogeneity inherent in the quantum dot ensembles, which are real objects in all the cases, makes it difficult to interpret the results in details. Consequently, most important are the common patterns that are observed on the background of this inhomogeneity. In the case of considered dispersions, the common patterns include, primarily, the dispersion PL in the visible region, which is characteristic for large molecules consisting of fused benzenoid rings. The feature is resulted from the nanosize metrics of the basic rGO fragments of all the dispersions. The second feature concerns the dependence of the position and intensity of PL spectra on the exciting light wavelength λ_{exc}. The feature follows from the first one and is caused by two facts: first, a selective excitation of a set of rGO ensembles, absorption characteristics of which mostly suit the excitation wavelength, and second, efficient donor–acceptor ability of rGO fragments leading to the formation of both homo and hetero charge-transfer complexes. The combination of molecular PL and donor–acceptor emission evidently depends on λ_{exc} due to varied overlapping of the relevant absorption spectra over the spectral range. At the same time, the formation of charge-transfer complexes involving rGO lays the foundation of nonlinear optical effects characteristic for GQDs.

Absorption spectra of the rGO fragments should be calculated in the framework of CI computational approaches. RHF based ZINDO/S is not applicable to the case once restricted to the spin polarization caused by electron correlation. The codes provide a reliable description of excited states of closed-shell molecules and applying to the studied 'bulk' molecules showed results well compatible with empirical observations concerning absorption and PL spectra of graphene oxides. When applied to open-shell framed rGO molecules, the tool revealed an unreal red shift of the absorption spectra as a consequence of the ignorance of the spin polarization of the molecules electronic states. Thus obtained absorption spectra strongly contradict the observation of GQDs UV absorption spectra and fluorescence in visible region. The discrepancy was explained by a severe underestimation of the HOMO-LUMO energy gap G_{RHF} of open-shell molecules in contrast to G_{UHF} predicted by UHF calculations. The latter values are well consistent with blue-green fluorescence of GQDs. Despite the evident inadequacy concerning the ZINDO/S application to open-shell molecules, the obtained results are full of important information and are highly required for the costly and time-consuming computational experiments with the tools of higher CI level in use to be optimally designed.

The main distinguishing GQD characteristic is surely its open-shell electronic system that is responsible for unique features related to GQDs not only in photonics, but in chemistry, biochemistry, biomedicine, and so forth. Accordingly, only framed graphene molecules are basic construction elements of GQDs. Among the latter, rGOs confidently take the first place. However, other framed molecules, such as members of the $C_{6n^2}H_{6n}$ family, an extended precursor $C_{96}H_{30}$ [72] or graphene nano-flakes derived from carbon nanotubes via three steps of pressing, homogenization and sonication-exfoliation processes [73] can be configured as GDQ stacks revealing spectral properties similar to those exhibited by synthetic and natural rGOs. As a whole, photonics of GQDs is a complex many-factor area. However, understanding the leading role of peculiar nanosize framed graphene fragments in all the processes involved is doubtlessly Ariadne's thread to find way in this complex labyrinth.

ACKNOWLEDGEMENTS

The authors (E.Sh. and N.P.) are thankful to the Ministry of Education and Science of the Russian Federation (the Agreement number 02.A03.21.0008) for financial support.

REFERENCES

[1] B. Trauzettel, D.V. Bulaev, D. Loss and G. Burkard // *Nat. Phys.* **3** (2007) 192.
[2] A. Güçlü, P. Potasz and P. Hawrylak // *Phys. Rev. B* **84** (2011) 035425.
[3] K.A. Ritter and J.W. Lyding // *Nat. Mater.* **8** (2009) 235.
[4] D. Pan, J., Zhang, Z. Li and M. Wu // *Adv. Mater.* **22** (2010) 734.

[5] J. Shen, Y. Zhu, C. Chen, X. Yang and C. Li // *Chem. Commun.* **47** (2011) 2580.
[6] Z.Z. Zhang, K. Chang and F.M. Peeters // *Phys. Rev. B* **77** (2008) 235411.
[7] V. Gupta, N. Chaudhary, R. Srivastava, G.D. Sharma, R. Bhardwaj and S. Chand // *J. Am. Chem. Soc.* **133** (2011) 9960.
[8] R. Liu, D. Wu, X. Feng and K. Müllen // *J. Am. Chem. Soc.* **133** (2011) 15221.
[9] Y. Li, Y. Hu, Y. Zhao, G. Shi, L. Deng, Y. Hou and L. Qu // *Adv. Mater.* **23** (2011) 776.
[10] L. Wang, S.-J. Zhu, H.-Y. Wang, S.N. Qu, Y.-L. Zhang, J.-H. Zhang, Q.-D. Chen, H.-L. Xu, W. Han, B. Yang and H.-B. Sun // *ACS Nano* **8** (2014) 2541.
[11] F. Liu, M.-H. Jang, H.D. Ha, J.-H. Kim, Y.-H. Cho and T.S. Seo // *Adv. Mat.* **25** (2013) 3657.
[12] S.K. Das, Y. Liu, S. Yeom, D.Y. Kim and C.I. Richards // *Nano Lett.* **14** (2014) 620.
[13] V. Štengl, S. Bakardjieva, J. Henych, K. Lang and M. Kormunda // *Carbon* **63** (2013) 537.
[14] L. Tang, R. Ji, X. Cao, J. Lin, H. Jiang, X. Li, K.S. Teng, C.M. Luk, S. Zeng, J. Hao and S.P. Lau // *ACS Nano* **6** (2012) 5102.
[15] L. Li, G. Wu, G. Yang, J. Peng, J. Zhao and J.-J. Zhu // *Nanoscale* **5** (2013) 4015.
[16] J. Peng, W. Gao, B.K. Gupta, Z. Liu, R. Romero-Aburto, L. Ge, L. Song, L.B. Alemany, X. Zhan, G. Gao, S.A. Vithayathil, B.A. Kaipparettu, A.A. Marti, T. Hayashi, J.-J. Zhu and P.M. Ajayan // *Nano Lett.* ***12*** (2012) 844.
[17] R. Ye, C. Xiang, J. Lin, Z. Peng, K. Huang, Z. Yan. N.P. Cook, C.-C. Hwang, G. Ruan, G. Ceriotti, A.-R.O. Raji, A.A. Martí and J.M. Tour // *Nat. Commun.* **4** (2013) 2943.
[18] E.F. Sheka and N.N. Rozhkova // *Int. J. Smart Nanomat.* **5** (2014) 1.
[19] X. Yan, B. Li and L.-S. Li // *Acc. Chem. Res.* **46** (2013) 2254.
[20] L.A. Ponomarenko, F. Schedin, M.I. Katsnelson, R. Yang, E.W. Hill, K.S. Novoselov and A.K. Geim // *Science* **320** (2008) 356.
[21] T.-F. Yeh, W.-L. Huang, C.-J. Chung, I.-T. Chiang, L.-C. Chen, C.-Y. Chang, W.-S. Su, C. Cheng, S.-J. Chen and H. Teng // *J. Phys. Chem. Lett.* **7** (2016) 2087.
[22] S. Zhu, J. Zhang, C. Qiao, S. Tang, Y. Li, W. Yuan, B. Li, L. Tian, F. Liu, R. Hu, H. Gao, H. Wei, H. Zhang, H. Sun and B. Yang // *Chem. Commun.* **47** (2011) 6858.
[23] H. Li, X. He, Z. Kang, H. Huang, Y. Liu, J. Liu, S. Lian, C.H. Tsang, X. Yang and S.T. Lee // *Angew. Chem. Int. Ed.* **49** (2010) 4430.
[24] X. Yan, B. Li, X. Cui, Q. Wei, K. Tajima and L.-S // *J. Phys. Chem. Lett.* **2** (2011) 1119.
[25] G. Eda, Y.-Y. Lin, C. Mattevi, H. Yamaguchi, X.-A. Chen, I.-S. Chen, C.-W. Chen and M. Chhowalla // *Adv. Mater.* **22** (2010) 505.
[26] X. Yan, X. Cui and L.S. Li // *J. Am. Chem. Soc.* **132** (2010) 5944.
[27] B.P. Biswal, D.B. Shinde, V.K. Pillai and R.Banerjee // *Nanoscale* **5** (2013) 10556.
[28] N.N. Rozhkova, *Shungite Nanocarbon* (Petrozavodsk: Karelian Research Centre of RAS, 2011), In Russian.
[29] E.F. Sheka and E.A. Golubev // *Tech. Phys.* **61** (2016) 1032.
[30] E.F. Sheka, I. Natkaniec, N.N. Rozhkova and K. Holderna-Natkaniec // *JETP Lett.* **99** (2014) 650.
[31] E.F. Sheka, I. Natkaniec, N.N. Rozhkova, E.Yu. Buslayeva, S.V. Tkachev, S.P. Gubin and V.P., Mel'nikov // *Nanosyst. Phys. Chem. Math.* **7** (2016) 71.
[32] Z. Gan, S. Xiong, X. Wu, T. Xu, X. Zhu, X. Gan, J. Guo, J. Shen, L. Sun and P.K. Chu // *Adv*. *Opt. Mater.* **1** (2013) 926.
[33] Z. Gan, H. Xu and Y. Hao // *Nanoscale* **8** (2016) 7794.
[34] B.S. Razbirin, N.N. Rozhkova, E.F. Sheka, D.K. Nelson and A.N. Starukhin // *J. Exp. Theor. Phys.* **118** (2014) 735.
[35] B.S. Razbirin, N.N. Rozhkova, E.F. Sheka, D.K. Nelson, A.N. Starukhin and A.S. Goryunov // *Nanosyst. Phys. Chem. Math.* **5** (2014) 217.
[36] T.A. Witten, In: *Soft Matter Physics,* ed. By M. Daoud and C.E. Williams (Springer-Verlag, Berlin Heidelberg, 999), p. 261.
[37] C. K.Chua and M. Pumera // *Chem. Soc. Rev.* **43** (2014) 291.
[38] B.S. Razbirin, E.F. Sheka, A.N. Starukhin, D.K. Nelson, P.A. Troshin and R.N. Lyubovskaya // *JETP Lett.* **87** (2008) 133.
[39] E.F. Sheka, B.S. Razbirin, A.N. Starukhin, D.K. Nelson, M.Yu. Degunov, P.A. Troshin and R.N. Lyubovskaya // *J. Exp. Theor. Phys.* **108** (2009) 738.
[40] E.F. Sheka, B.S. Razbirin, A.N. Starukhin, D.K. Nelson, M.Yu. Degunov, R.N. Lyubovskaya and P.A. Troshin // *J. Nanophoton.* **3** (2009) 033501.

[41] P. Heritage and A.M. Glass , In: *Surface Enhanced Raman Scattering*, ed. by R.K. Chang and T.E. Furtak (Plenum Press: NY and London,1982), p.391.
[42] E.F. Sheka // *Nanosci. Nanothech. Lett.* **3** (2011) 34.
[43] B.S. Razbirin, N.N. Rozhkova and E.F. Sheka, In: *Graphene Science Handbook: Electrical and Optical Properties*, Vol.3, ed. by M. Aliofkhazraei, N. Ali, W.I. Miln, C.S., Ozkan, S. Mitura and J. Gervasoni (CRC Press, Taylor and Francis Group, Boca Raton, 2016), p. 425.
[44] M.A. Budyka, E.F. Sheka and N.A. Popova // *Cond. Mat. Mater. Sci.* (2017) *arXiv*:1702.07197 [cond-mat.mtrl-sci].
[45] E.F. Sheka, In: *Graphene Science Handbook: Mechanical and Chemical Properties*, Vol.4., ed. by M. Aliofkhazraei, N. Ali, W.I. Miln, C.S. Ozkan, S. Mitura and J. Gervasoni (CRC Press, Taylor and Francis Group, Boca Raton, 2016), p. 312.
[46] E.F. Sheka and N.A. Popova //*J. Mol. Model.* **18** (2012) 3751.
[47] E.F. Sheka and N.A. Popova // *Phys. Chem. Chem. Phys.* **15** (2013) 13304.
[48] E.F. Sheka // *J. Str. Chem.* 47 (2006) 593.
[49] E.F. Sheka // *Cond. Mat. Mater. Sci.* (2016), arXiv:1611.02696.
[50] E. F. Sheka, In: *Advances in Quantum Methods and Applications in Chemistry, Physics, and Biology*, ed. by A. Tadjer, E.J. Brändas, J. Maruani and G. Delgado-Barrio, (Springer, Switzerland, 2016), p. ?????.
[51] J. Ridley and M. Zerner // *Theor. Chem. Acta* **32** (1973) 111.
[52] M. J. Frisch, G. W. Trucks, H. B. Schlegel, et.al., *Gaussian 09, Revision B.01* (Gaussian, Inc., Wallingford CT, 2010).
[53] A. Dreuw and M. Head-Gordon // *Chem. Rev*. **105** (2005) 4009.
[54] S. Grimme and M. Parac // *Chemphyschem.* **3** (2003) 292.
[55] K. Lopata, R. Reslan, M. Kowalska, D. Neuhauser, N. Govind and K. Kowalski // *J. Chem. Theory Comput*. **7** (2011) 3686.
[56] L.H. Starcke, M. Wormit and A. Dreuw // *J. Chem. Phys*. **130** (2009) 024104.
[57] J. Wenzel, M. Wormit and A. Dreuw // *J. Chem. Theory Comput*. **10** (2014) 4583.
[58] H. Nakata, D.G. Fedorov, T. Nagata, S. Yokojima, K. Ogata and S. Nakamura // *J. Chem. Phys*. **137** (2012) 044110.
[59] H. Nakata, D.G. Fedorov, S. Yokojima, K. Kitaura, M. Sakurai and S. Nakamura // *J. Chem. Phys.* **140** (2014) 144101.
[60] J. Guan, M.E. Casida and D.R. Salahub // *J. Mol. Struct. (Theochem)* **527** (2000) 229.
[61] *UV Spectroscopy : Techniques, Instrumentation, Data Handling*, ed. by. B.J. Clark, T. Frost and M.A. Russell (Chapman & Hall: London New York, 1993).
[62] J. Shang, L. Ma, J. Li, W. Ai, T. Yu and G.G. Gurzadyan // *Sci. Rep*. **2** (2012) 792.
[63] J.R. Rani, J. Lim, J. Oh, J.-W. Kim,H.S. Shin, J.H Kim, S. Lee and S.C. Jun // *J. Phys. Chem. C* **116** (2012) 19010.
[64] S. Vempati and T. Uyar // *Phys. Chem. Chem. Phys.***16** (2016) 21183.
[65] D.-H. Chae, T. Utikal, S. Weisenburger, H. Giessen, K. Klitzing, M. Lippitz and J. Smet // *Nano Lett*.**11** (2011) 1379.
[66] S. Mohajer, M.H.M. Ara and L. Serahatjoo // *Journ Nanophot*. **10** (2016) 036014.
[67] S. Zhu, J. Zhang, X. Liu, B. Li, X. Wang, S. Tang, Q. Meng, Y. Li, C. Shi and R. Hu // *RSC Adv*. **2** (2012) 2717.
[68] Y. Kawashima, T. Hashimoto, H. Nakano and K. Hirao // *Theor.Chem. Acc.* **102** (1999) 49.
[69] E.F. Sheka, (2017), Private communication.
[70] C. Cocchi, D. Prezzi, A. Ruini, M. Caldas and E. Molinari // *J. Phys. Chem. Lett.* **2** (2011) 1315.
[71] E.F. Sheka, In: *Carbon Materials: Chemistry and Physics: Vol. 7, Topological Modelling of Nanostructures and Extended Systems*, ed. by A.R. Ashrafi, F. Cataldo, A. Iranmanesh and O. Ori (Springer: Berlin, 2013), p. 137.
[72] B. Yuana, X. Suna, J. Yana, Z. Xie, P. Chen and S. Zhou // *Phys. Chem. Chem. Phys*. **18** (2016) 25002 .
[73] P. Lin, Y. Chen, K. Hsu, T.N. Lin, K. Tung, J.L. Shen and W. Liu // *Phys. Chem. Chem. Phys.* **19** (2017) 6338.
[74] P. Wagner, C. P. Ewels, J.-J. Adjizian, L. Magaud, P. Pochet, S. Roche, A. Lopez-Bezanilla, V.V. Ivanovskaya, A. Yaya and M. Rayson //*J. Phys. Chem. C* **117** (2013) 26790.